University of Crete, Department of Physics

I.E.S.L. - FO.R.T.H.

Polarization Spectroscopy Group

Bachelor Thesis

"Measurement of Weak Chiral Optical Rotation of Methyl Lactate Vapor via Cavity Enhanced Polarization Spectroscopy"

Name: Artemis Linaraki

Supervisor: Prof. T. Peter Rakitzis

Herakleion, Crete – 2022

FOUNDATION FOR RESEARCH AND TECHNOLOGY - HELLAS

Contents

Table of Figures

Abstract

The purpose of this thesis is the demonstration of the utilization of a polarimeter developed to measure extremely weak optical rotations with unprecedented sensitivity. In this work, the samples of interest were chiral vapors. More specifically, we focused on methyl lactate. The measurements were based on a Cavity Ring-Down scheme, employing two signal reversals, allowing us to obtain results for the absolute optical rotation of this gaseous sample. We acquired measurements with a sensitivity of ~50 μdeg/√Hz, while state-of-the-art commercial polarimeters can only reach a sensitivity down to ~5 mdeg/√Hz. This work opens the way for measurements of the chiral optical rotation of ethyl-1-d-benzene, which is expected to have small optical activity, as it is chiral only due to isotopic substitution.

1: Theory

1.1 Gaussian Beams

The mathematical model which represents the distribution of the electric field of propagating light is what we refer to as Gaussian beam. The vast majority of optical beams that propagate in free space can be described as transverse electric and magnetic (~TEM), which means that the field components are perpendicular to the propagation direction. To obtain the aforementioned model concerning beams created by lasers, we engage an approximate analytic solution to the wave equation under determined conditions.

We begin with the form of the electric field **E**. The wave equation in this case is:

$$\nabla^2 \boldsymbol{E} - \frac{1}{c^2} \cdot \frac{\partial^2 \boldsymbol{E}}{\partial t^2} = 0 \quad \textbf{(1.1.1)}$$

We know that the field propagates with a velocity of c in free space. Therefore, the solution we are searching for, must be of the form: $E(x,y,z) = E_0 \psi(x,y,z) e^{-i(kz-\omega t)}$ **(1.1.2)**

We now replace **(1.1.2)** in **(1.1.1)**: $\frac{\partial^2 \psi}{\partial x^2} + \frac{\partial^2 \psi}{\partial y^2} - i2k\frac{\partial \psi}{\partial z} = 0$ **(1.1.3)**, where the second derivative is excluded, since the variation with respect to the phase factor is very slow.

The solution of **(1.1.3)** gives **E**.

The magnetic field **B**, can be obtained via solving: $\nabla \times \boldsymbol{B} = \frac{-\partial \boldsymbol{E}}{\partial t}$ **(1.1.4)**.

The $TEM_{m,p}$ modes can thus be constructed by combining the results of **(1.1.3)** & **(1.1.4)**:

$$TEM_{m,p}(\boldsymbol{r},t) = E_{m,p} H_m\left(\frac{\sqrt{2}x}{w(z)}\right) H_p\left(\frac{\sqrt{2}y}{w(z)}\right) \frac{w_0}{w(z)} e^{\frac{-r^2}{w^2(z)}} e^{-i[kz-(1+m+p)\tan^{-1}(\frac{z}{z_0})]} e^{-i\frac{kr^2}{2R(z)}} \quad \textbf{(1.1.5)}$$

where $r^2=x^2+y^2$, and (x,y,z) are the Cartesian coordinates. We have considered z to be the propagation direction.

Schematically, the cross sections of some of the first $TEM_{m,p}$ modes are:

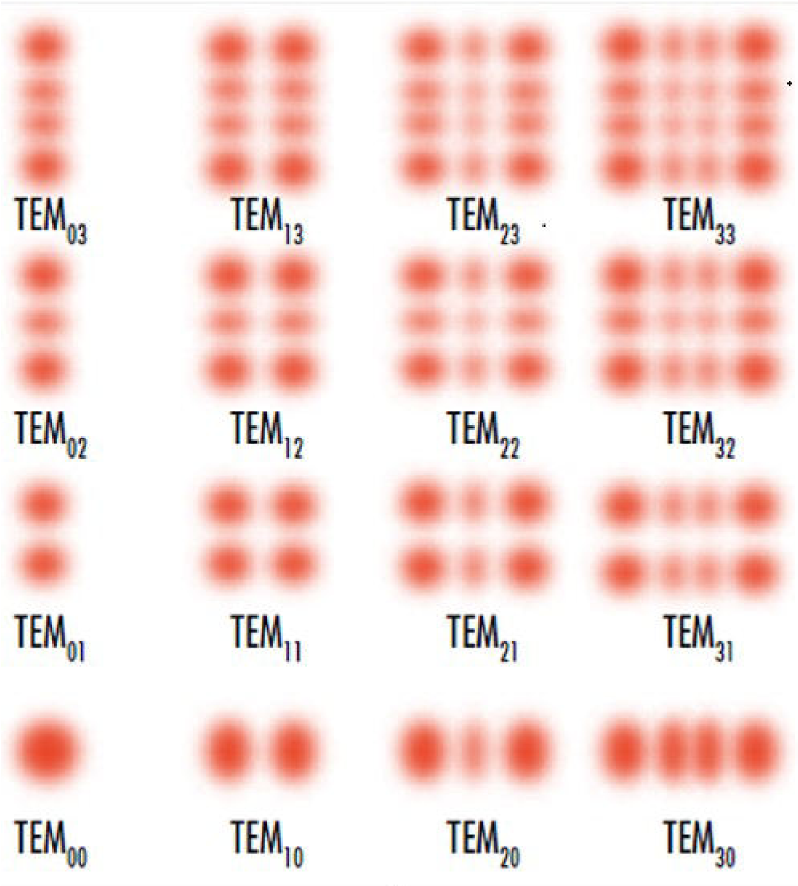

Figure 1: Cross sections of $TEM_{m,p}$ modes

Image from: https://www.edmundoptics.com.tw/knowledge-center/application-notes/lasers/laser-resonator-modes/

Furthermore:

- H_m & H_p are the Hermite polynomials of order m & p respectively
- w(z) is the spot size, or the diameter of the beam that can be observed at any point on the z-axis, given by: $w(z)=w_0\sqrt{1+(\frac{z}{z_0^2})}$ **(1.1.6)**
- w_0 is the minimum spot size (or waist), meaning the diameter of the beam at the focus
- R(z) is the radius of curvature, given by: $R(z)=z[1+(\frac{z}{z_0})^2]$ **(1.1.7)**
- z_0 is the Rayleigh range, a constant showing the distance from the focus where approximately $w(z)=w_0$, given by: $z_0=\frac{\pi w_0^2}{\lambda_0}$ **(1.1.8)** where λ_0 is the wavelength of the light in free space

The quantities mentioned above are included in the following Figure, in which 2θ is the total angular spread:

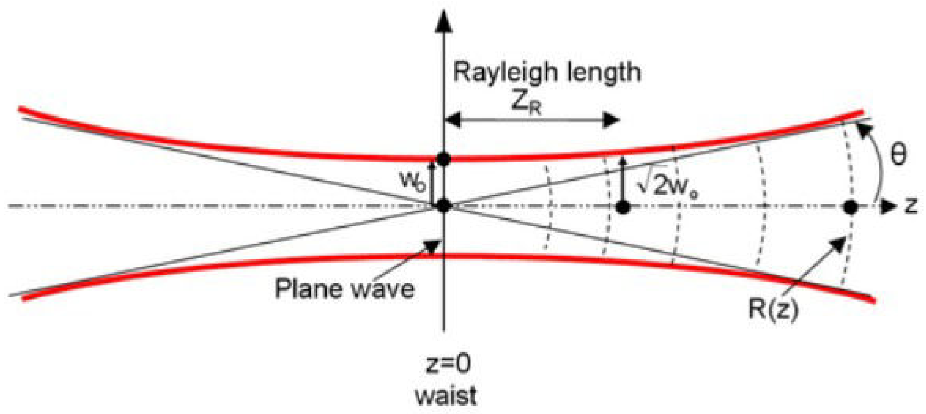

Figure 2: The width of a Gaussian beam as a function of z along the beam

Image from: http://www.optique-ingenieur.org/en/courses/OPI_ang_M01_C03/co/Contenu_08.html

1.2 Polarization

The electric field of light as an electromagnetic wave oscillates perpendicularly to the propagation direction. Light is considered to be unpolarized if the direction of its electric field fluctuates randomly in time. In the case of a well defined direction of the electric field, light is considered to be polarized. Lasers are the most common source of polarized light.

There are three categories of polarization depending on the orientation of the electric field of polarized light:

1. *Linear* – **E** is confined to a single plane along the propagation direction.

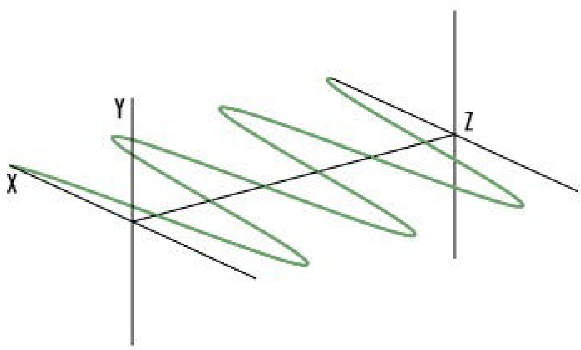

Figure 3: The electric field of linearly polarized light, confined to the x-z plane, along the propagation direction

Image from: https://www.edmundoptics.com/knowledge-center/application-notes/optics/introduction-to-polarization/

2. *Circular* – **E** consists of two linear components that are perpendicular to each other, equal in amplitude, but have a phase difference of π/2. As a result, **E** rotates in a circle around the propagation direction. It is called left- or right- hand circularly polarized light (~ LCP/RCP), depending on the direction of rotation.

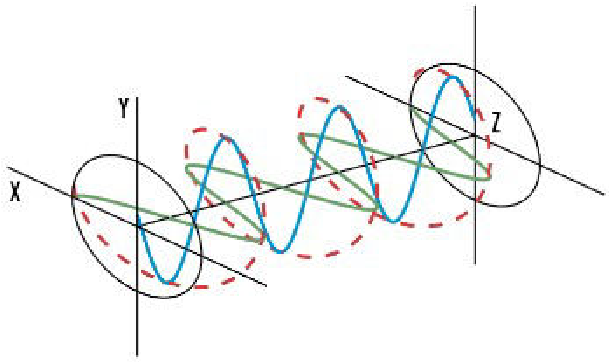

Figure 4: The electric field of circularly polarized light

Image from: https://www.edmundoptics.com/knowledge-center/application-notes/optics/introduction-to-polarization/

3. *Elliptical* – **E** describes an ellipse, which is a result of the combination of two linear components with different amplitudes and/or a phase difference that is not π/2.

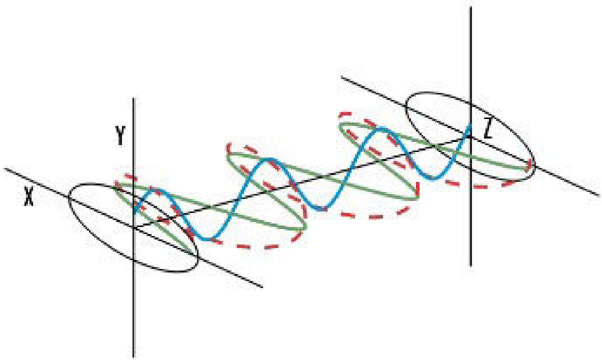

Figure 5: The electric field of elliptically polarized light

Image from: https://www.edmundoptics.com/knowledge-center/application-notes/optics/introduction-to-polarization/

A noteworthy fact is that elliptical polarization is the most general description of polarized light. Linear and circular polarized light are viewed as special cases of this general polarization type.

Studying and manipulating the polarization of light can get difficult. However, there are certain tools that have been developed so as to simplify the process. An outstanding example is Jones Calculus, which we will further discuss further below.

1.3 Jones Calculus

In this context, Jones vectors represent polarized light and Jones matrices represent the various linear optical elements, such as polarizers and phase retarders. When light traverses such an element, the resulting polarization of the emerging light can be calculated by the product of the Jones matrix of the optical element and the Jones vector of the incident light. It is critical to remember that Jones Calculus can be utilized only in the case of fully polarized light. Concerning this work, light is very close to satisfying this condition, and consequently, we consider Jones Calculus to be applicable.

Firstly, we designate the electric field:

$$\boldsymbol{E}=\begin{pmatrix} E_x(t) \\ E_y(t) \end{pmatrix}=\begin{pmatrix} E_{0x}e^{-i(kz-\omega t-\varphi_x)} \\ E_{0y}e^{-i(kz-\omega t-\varphi_y)} \end{pmatrix}\sim\begin{pmatrix} E_{0x}e^{i\varphi_x} \\ E_{0y}e^{i\varphi_y} \end{pmatrix} \quad \textbf{(1.3.1)}$$

The Jones vectors that describe the three different polarization types are:

1. Linearly polarized: $\boldsymbol{E}_{linear}=\begin{pmatrix} a \\ b \end{pmatrix}$ **(1.3.2)**

For instance, if the polarization is in the x direction:
$\boldsymbol{E}_{linear}=\begin{pmatrix} 1 \\ 0 \end{pmatrix}$ **(1.3.3)**, also called horizontal.
If it is in the y direction: $\boldsymbol{E}_{linear}=\begin{pmatrix} 0 \\ 1 \end{pmatrix}$ **(1.3.4)**, called vertical.

2. Circularly polarized: $\boldsymbol{E}_{circular}=\frac{1}{\sqrt{2}}\begin{pmatrix} 1 \\ \pm i \end{pmatrix}$ **(1.3.5)**, where the (+) refers to LCP and the (-) to RCP.

3. Elliptically polarized: $\boldsymbol{E}_{linear}=\begin{pmatrix} a \\ be^{i\varphi} \end{pmatrix}$ **(1.3.6)**.

The matrix describing the polarization rotation is the following:

$$R(\theta)=\begin{pmatrix} cos\theta & -sin\theta \\ sin\theta & cos\theta \end{pmatrix} \quad \textbf{(1.3.7)}$$

When it comes to the (2×2) Jones matrices that describe optical elements, we have:

- Linear polarizers: Horizontal: $\begin{pmatrix} 1 & 0 \\ 0 & 0 \end{pmatrix}$ **(16)** Vertical: $\begin{pmatrix} 0 & 0 \\ 0 & 1 \end{pmatrix}$ **(1.3.8)**

  Angle θ: $\begin{pmatrix} \cos^2\theta & cos\theta sin\theta \\ cos\theta sin\theta & \sin^2\theta \end{pmatrix}$ **(1.3.9)**

➢ Quarter-wave plates:

Fast axis horizontal: $e^{\frac{-i\pi}{4}}\begin{pmatrix}1 & 0\\ 0 & i\end{pmatrix}$ **(1.3.10)** Fast axis vertical: $e^{\frac{i\pi}{4}}\begin{pmatrix}1 & 0\\ 0 & -i\end{pmatrix}$ **(1.3.11)**

Fast axis at angle θ: $e^{\frac{-i\pi}{4}}\begin{pmatrix}\cos^2\theta + isin^2\theta & (1-i)\,sin\theta cos\theta\\ (1-i)\,sin\theta cos\theta & \sin^2\theta + icos^2\theta\end{pmatrix}$ **(1.3.12)**

➢ Half-wave plates: $e^{\frac{-i\pi}{2}}\begin{pmatrix}\cos^2\theta - \sin^2\theta & 2\,sin\theta cos\theta\\ 2\,sin\theta cos\theta & \sin^2\theta - \cos^2\theta\end{pmatrix}$ **(1.3.13)**, fast axis at angle θ

As mentioned above, the multiplication of the Jones vectors representing the incident light and matrices such as the ones listed here, leads to the calculation of the final effect on the light polarization for any given optical elements compilation. We should take into consideration that the integrated intensity measurement does not correspond to the field itself. It is connected to the surface of the given system for the detection of light.

1.4 Optical Cavities

An optical cavity is an arrangement of optical components, usually high reflectivity mirrors, which enables a beam of light to circulate in a close path again and again. We are particularly interested in the mirror reflectivity, since we are aiming for a high amount of round trips. At the same time, after each round trip, there is a small, but measurable, light leakage that is detected by a diode system.

Cavities can be constructed in various setups, all of which could be discerned between two main types:

- *Standing* - In this case, light bounces back and forth between two end mirrors

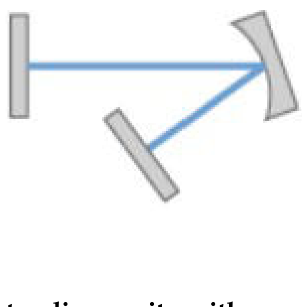

Figure 6: A simple standing cavity with a curved folding mirror

- *Running* - This category has no end mirrors, and the light can circulate in two different directions

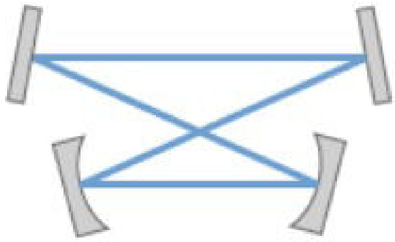

Figure 7: A four-mirror bow-tie running cavity

The main difference is the amount of times light traverses every cavity element. That number is 2 in the first case, and 1 in the second. In either case, the cavity can include additional optical components that are traversed in every round trip.

One can realize the significant applicability of cavities when attempting to measure light absorption in low absorbance samples. A single pass measurement in this case would not be the solution, since the intensity signal would be altered too vaguely to detect.

We shall now examine the effect of a cavity on the light intensity in such a situation. For instance, in a two-mirror cavity, supposedly of mirrors M_1 and M_2, with mirror reflectivities R_1 and R_2 respectively, where a light pulse of initial intensity I_0 is fired and enters the cavity through M_1, we could detect the light intensity signal by setting a photodetection system right after M_2. As discussed previously, due to the fact that $R_1, R_2 \neq 1$, after each round trip, there will be a detectable leakage of light. After n round trips, the light intensity will have be of the form:

$$I_n = (R_1 \cdot R_2)^n I_0 = S^n I_0 = S I_{n-1} \quad \textbf{(1.4.1)}$$

In order to construct a formula where I is a function of time, we need to determine the time it takes for light to perform a complete round trip, called τ_{rt}. The lengths of the most commonly used cavities are the order of a meter. As a result, $\tau_{rt} \sim$ ns.

If we set $n = \frac{t}{\tau_{rt}}$, **(1.4.2)** becomes continuous: $I(t) = S I(t - \tau_{rt})$ **(1.4.3)**.

We now apply Taylor expansion, which leads to: $\frac{dI}{dt} = -\frac{1-S}{\tau_{rt}} I$ **(1.4.4)**.

At this point, we can define $\tau_{rd} = \frac{\tau_{rt}}{1-S}$ **(1.4.5)**, where τ_{rd} is a useful quantity called ringdown time.

We substitute **(1.4.5)** to **(1.4.4)**: $\frac{dI}{dt} = -\frac{1}{\tau_{rd}} I$ **(1.4.6)**,

which is a simple differential equation with a solution of the form: $I(t) = I_0 e^{-\frac{t}{\tau_{rd}}}$ **(1.4.7)**

One final step is to multiply the light intensity that traverses M_2 with its transmissivity, T_2:

$$I(t)=T_2 I_0 e^{-\frac{t}{\tau_{rd}}} \quad \textbf{(1.4.8)}$$

We get a similar result in the case of a four-mirror bow-tie cavity. The only difference is found in τ_{rd}, since $S=R_1R_2R_3R_4$, where R_i is the reflectivity of the i^{th} mirror, and here, i=1,..,4. Moreover, the final result in this case is multiplied with the transmissivity T_4 of the fourth mirror. Thus:

$$I(t)=T_4 I_0 e^{-\frac{t}{\tau_{rd}}} \quad \textbf{(1.4.9)}, \text{ where } \quad \tau_{rd}=\frac{\tau_{rt}}{1-R_1 R_2 R_3 R_4} \quad .$$

Adding a sample of absorbance A into the cavity leads us to the following results:

$$I_n=(R_1 \cdot R_2 A)^n I_0=S^n{}_A I_0=S_A I_{n-1} \quad \textbf{(1.4.10)} \text{ and } \quad \frac{dI}{dt}=-\frac{1-S_A}{\tau_{rt}} I \Leftrightarrow \frac{dI}{dt}=-\frac{1}{\tau_{rd_A}} I \quad \textbf{(1.4.11)}.$$

It becomes quite clear that different ringdown times are subsequent to different absorbances. It is now fairly easy to measure the absorbance:

$$A=\frac{1-\frac{\tau_{rt}}{\tau_{rd,A}}}{1-\frac{\tau_{rt}}{\tau_{rd}}} \quad \textbf{(1.4.12)}$$

The figure below includes three examples of ringdown signals:

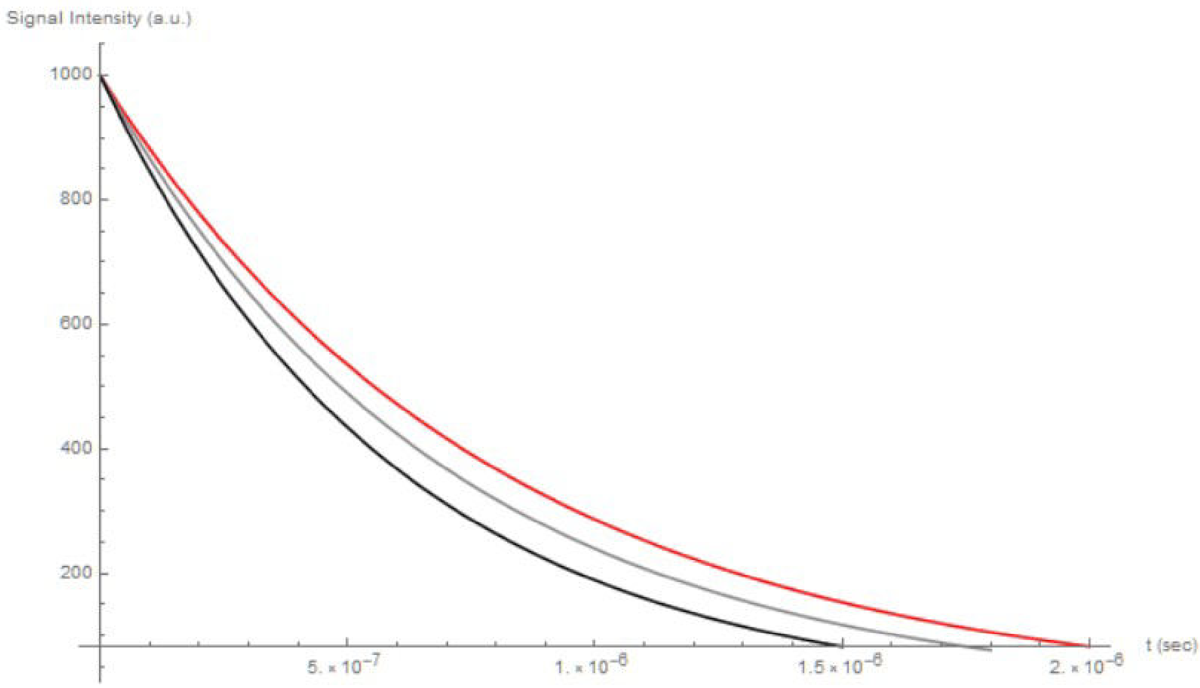

Figure 8: Ringdown signals with a difference in ringdown times

The red curve represents the signal recorded while the cavity is empty, while the gray and black curves represent the signal obtained when media of absorbances A_1 and A_2, where $A_1<A_2$, respectively are inserted into the cavity.

The signals of our studies are characterized by the form of the next figure:

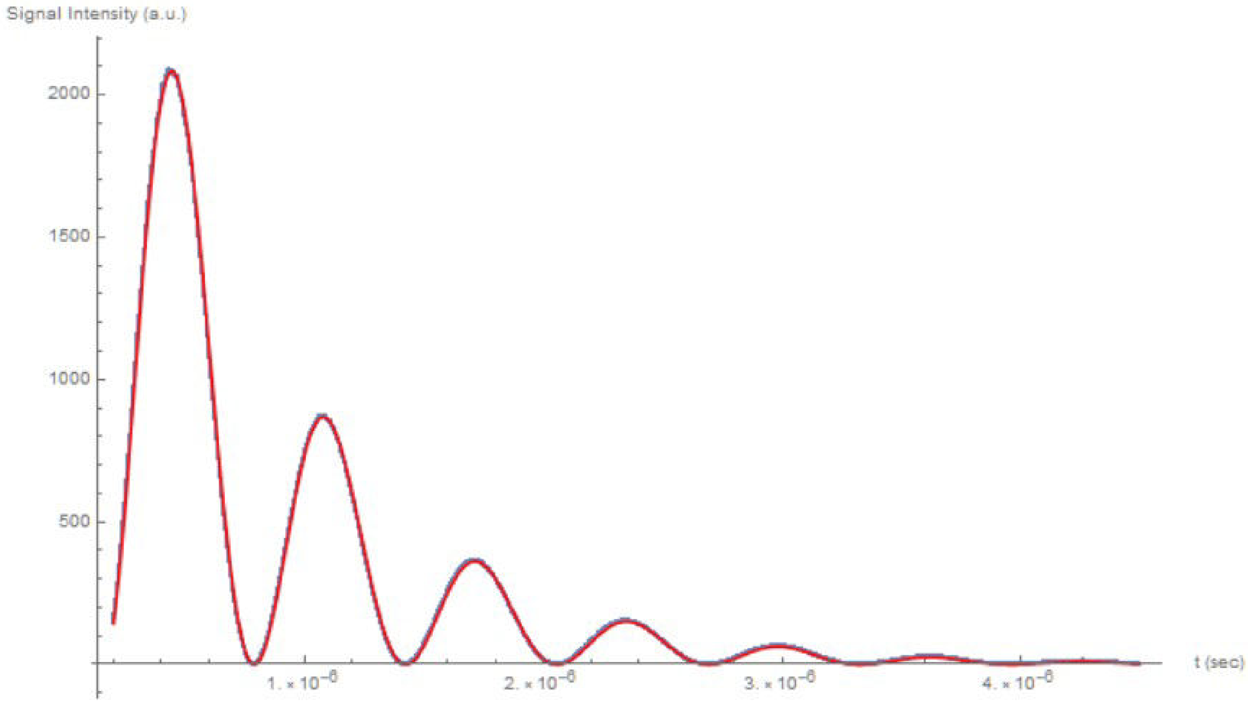

Figure 9: Ringdown signal with an optically active medium inside the cavity

That is because our samples of interest do not just absorb some portion of the light when added into our four-mirror cavity. They additionally generate a rotation to the polarization of light. This is a rotation of an angle φ per pass, and it cannot be observed unless we insert a linear polarizer in the intermediate space between M_4 and the photodetection system.

This type of intensity signals is described by:

$$I(t)=T_4 I_0 e^{-\frac{t}{\tau_{rd}}}\cos^2\left(\frac{\varphi t}{\tau_{rt}}\right) \quad \textbf{(1.4.13)}.$$

Substituting φ/τ_{rt} with the angular frequency, we get:

$$I(t)=T_4 I_0 e^{-\frac{t}{\tau_{rd}}}\cos^2(\omega t) \quad \textbf{(1.4.14)}.$$

1.5 Mode Matching

An important aspect of the nature of light that we must keep in mind when constructing an optical cavity, is the beam's tendency to broaden. This is even more critical when the path length is significantly greater than the Rayleigh length. Cavities such as the ones we usually work with are built with the purpose of reaching several dozens of round trips. Thus, the path length of the beam reaches the order of a kilometer, which naturally leads the beam broadening to a point where its waist would be quite larger than the surface of the cavity mirrors. As a result, almost all of the beam light would escape.

We come to the realization that a cavity must be carefully mode matched to be functional. In our case, that means the curvature radius of the beam must be matched to the curvature radius at the cavity mirrors. The beam originating from the laser must be mode matched before it even enters the cavity. This is achieved by including suitable lenses in specific distances between the laser and the cavity. That way, the beam waist coincides with the position of the flat input coupler, so the curvatures of the beam and the coupler match at their meeting point. The interior of the cavity includes both flat and spherical mirrors to ensure mode matching occurs at each point.

In general, a cavity mode is a field distribution that reproduces itself in relative shape and in relative phase after a round trip through the system. We can use this definition and the application of the so called ABCD law in order to find the characteristic modes of an optical cavity.

We know a light wave **E** can be represented by a column vector and the effect of an optical component on **E** has the form of a 2×2 matrix.

We need to construct the matrix representing a round trip through the cavity. To that end, we make the assumption that the characteristic modes of our cavity are the Hermite-Gaussian beams, and we demand that the complex beam parameter q repeats itself after each round trip.

Note that q is given by: $\frac{1}{q}=\frac{1}{R}-i\frac{\lambda}{\pi w^2}$ **(1.5.1)**

In our case, we utilize the following matrices: $P=\begin{pmatrix}1 & d\\ 0 & 1\end{pmatrix}$ **(1.5.2)** and $M=\begin{pmatrix}1 & 0\\ -\frac{2}{R} & 1\end{pmatrix}$ **(1.5.3)**, which represent the propagation of light in free space and its reflection by a mirror, respectively.

We also have the curvature radii of our four mirrors, being R_1, R_2, R_3, and R_4. In addition, the longer cavity arm has a length of d_1 and the shorter has a length of d_2. All of the components needed for the construction of the ABCD matrix characterizing our system are now assembled. Therefore:

$$M_{tot}=M(R_1)P(d_1)M(R_2)P(d_2)M(R_3)P(d_1)M(R_4)P(d_2)\Leftrightarrow M_{tot}=\begin{pmatrix}A & B\\ C & D\end{pmatrix} \quad \textbf{(1.5.4)}.$$

By acting on **E** with M_{tot}, we get the position and the inclination of the beam after each round trip. We recall that q must transform into itself after a round trip, which means the condition below must be satisfied:

$q(z_1+round\,trip)=q(z_1)$ **(1.5.5)**, where $q(z_1)$ is the complex parameter of the initial beam.

We now apply the ABCD law to find the left part of the equation:

$$q(z_1+round\,trip)=\frac{Aq(z_1)+B}{Cq(z_1)+D}\Leftrightarrow\frac{1}{q(z_1)}=\frac{C+D\frac{1}{q(z_1)}}{A+B\frac{1}{q(z_1)}} \quad \textbf{(1.5.6)}$$

M_{tot} must be unitary. Thus, solving for $1/q(z_1)$, we are led to the following system:

$B(\frac{1}{q^2})+2(\frac{A-D}{2})(\frac{1}{q})-C=0$ **(1.5.7)** and $AD-BC=1$ **(1.5.8)**.

Every set of the parameters A, B, C, and D that satisfy **(1.5.7)** & **(1.5.8)**, leads to a different array of mirrors in certain distances that ensure the occurrence of mode matching. Needless to say this is a mathematical approach, and it is practically impossible to have a perfectly mode matched optical cavity in realistic setups.

1.6 Birefringence

In general, birefringence is an optical property related to a difference in the refractive index of a material. We discern two types of birefringence:

- *Linear* - The refractive index depends on the polarization direction.

  There are two perpendicular axes, the fast and slow axes, and each one is characterized by a refractive index, n_f and n_s respectively. We will examine how a beam of polarized light is affected when traversing a linearly birefringent medium. If the light is initially polarized at an angle θ, with respect to the fast axis, coinciding with the horizontal axis, we have:

  $\boldsymbol{E}=\begin{pmatrix}cos\theta\\ sin\theta\end{pmatrix}$ **(1.6.1)**, which can be analyzed into: $\boldsymbol{E}=cos\theta\,\boldsymbol{E_f}+sin\theta\,\boldsymbol{E_s}$ **(1.6.2)**,

  where $\mathbf{E_f}$ and $\mathbf{E_s}$ are the components of the fast and slow axis of the polarization. After traversing a certain distance inside the medium, let's say d, **E** becomes:

  $$\boldsymbol{E}'=cos\theta\,\boldsymbol{E_f}e^{ikn_f d}+sin\theta\,\boldsymbol{E_s}e^{ikn_s d}\Leftrightarrow\boldsymbol{E}'=e^{ikn_f d}\begin{pmatrix}cos\theta\\ sin\theta e^{ik(n_s-n_f)d}\end{pmatrix}\Leftrightarrow\boldsymbol{E}'\sim\begin{pmatrix}cos\theta\\ sin\theta e^{i\varphi}\end{pmatrix} \quad \textbf{(1.6.3)},$$

  where φ is the phase picked up by the electric field during the aforementioned process.

Thus, we understand that linear birefringence causes a fundamental change in the polarization of light: linearly polarized light transforms to elliptically polarized light after traversing a linearly birefringent medium.

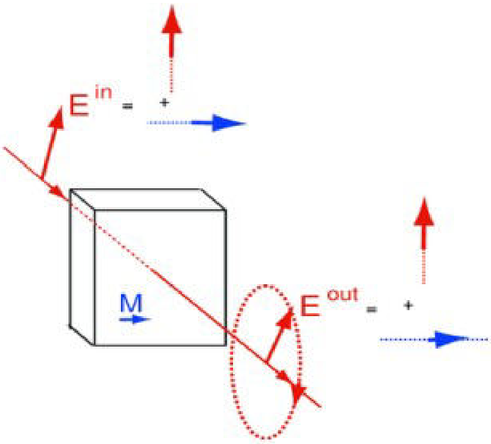

Figure 10: The effect of linear birefringence

Image from: https://www.researchgate.net/figure/a-Magneto-optical-Faraday-effect-b-Magnetic-linear-birefringence_fig3_254877783

- *Circular* – The phenomenon in which there is a difference between the refractive indices of a material for right- and left- circularly polarized light.

Suppose the refractive index of the right-circularly polarized light is represented by n_+ and n_- is the corresponding characteristic for the left-circularly polarized light. The effect of circular birefringence on a beam of light is examined in the next few steps. Firstly, we consider the light polarization is along the x-axis, so:

$\boldsymbol{E}=\begin{pmatrix}1\\0\end{pmatrix}$ **(1.6.4)** that can be analyzed into: $\boldsymbol{E}=\frac{1}{\sqrt{2}}[\boldsymbol{E}_{rcp}+\boldsymbol{E}_{lcp}]$ **(1.6.5)**, where:

$\boldsymbol{E}_{rcp}=\frac{1}{\sqrt{2}}\begin{pmatrix}1\\-i\end{pmatrix}$ **(1.6.6)** and $\boldsymbol{E}_{lcp}=\frac{1}{\sqrt{2}}\begin{pmatrix}1\\i\end{pmatrix}$ **(1.6.7)**.

Again, we are looking for the form of the electric field after the beam has covered a certain distance inside a circularly birefringent medium:

$$\boldsymbol{E}'=\frac{1}{\sqrt{2}}[\boldsymbol{E}_{rcp}e^{ikdn_{+¿}}+\boldsymbol{E}_{lcp}e^{ikdn_{-¿}}]\Leftrightarrow\boldsymbol{E}'=e^{ikd(n_{+¿}+n_{-¿})}\begin{pmatrix}\cos[\frac{k(n_{+¿}-n_{-¿})}{d}]\\ \sin[\frac{k(n_{+¿}-n_{-¿})}{d}]\end{pmatrix}\quad\textbf{(1.6.8)}.$$

We therefore deduct that the effect of circular birefringence on linearly polarized light is the rotation of the initial electric field by an angle $k(n_+ - n_-)/d$.

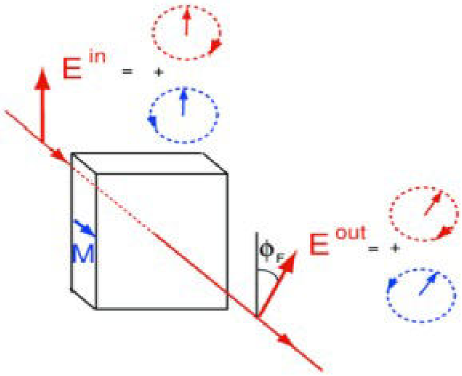

Figure 11: The effect of circular birefringence

Image from: https://www.researchgate.net/figure/a-Magneto-optical-Faraday-effect-b-Magnetic-linear-birefringence_fig3_254877783

There are at least two sources of linear and one source of circular birefringence that can affect our optical setup.

The main source of linear birefringence in our cavity is a CeF_3 magneto-optical crystal. That happens if the beam does not propagate through the crystal in a path that is parallel to the latter's axis, and it can be handled via proper alignment. Linear birefringence can also be introduced if the angle of the incident beam on a mirror is greater than the critical angle. Since our mirrors are multi-layered, this problem can be dealt with if we ensure the angles of incidence are quite low, at an order of a few degrees, during the process of designing the cavity.

A potential source of circular birefringence is the non-planarity that can occur if any of our cavity's four mirrors is somehow found off the plane that is defined by the remaining three.

Additionally, there are sources of birefringence that cannot be controlled so easily, such as particles of dust in the cavity environment that interfere with the beam of light, or vibrations caused by mechanic or human motions taking place closely from the cavity.

As one could imagine, avoiding every source of birefringence is an unrealistic expectation. However, its effects can be minimized, if we include significant Faraday rotations in our measuring method.

1.7 Faraday Effect

The Faraday effect is a magneto-optical phenomenon that causes the rotation of the polarization plane of a light beam traversing a material, due to the existence of a magnetic field. It is named after Michael Faraday, who discovered that the polarization plane is rotated when the light path and the direction of the applied magnetic field are parallel.

If a light beam traverses a medium of length l and the applied magnetic field is of the form $\boldsymbol{B}(z)=f(z)\hat{z}$, supposing the propagation direction is along the z-axis, the Faraday rotation can be calculated by: $\varphi_F=\int_0^l Vf(z)dz$, **(1.7.1)**

where V is the Verdet constant, a property of the medium, given by: $V=\frac{dn}{d\lambda}\frac{\lambda}{2c^2}\frac{q}{m}$ **(1.7.2)**

and:

- n is the refractive index of the medium
- q is the electron charge
- m is the electron mass

It is understandable that the magnitude of the rotation depends upon the strength of the magnetic field, the nature of the transmitting medium, and the Verdet constant.

The most astonishing characteristic of this effect, is that the direction of the rotation it causes is the same as the direction of current flow in the wire of the electromagnet. Therefore, the sign of the Faraday rotation is not affected by a change in the light's propagation direction. The only parameter that can cause a change in the sign of φ_F, is the applied magnetic field. Schematically:

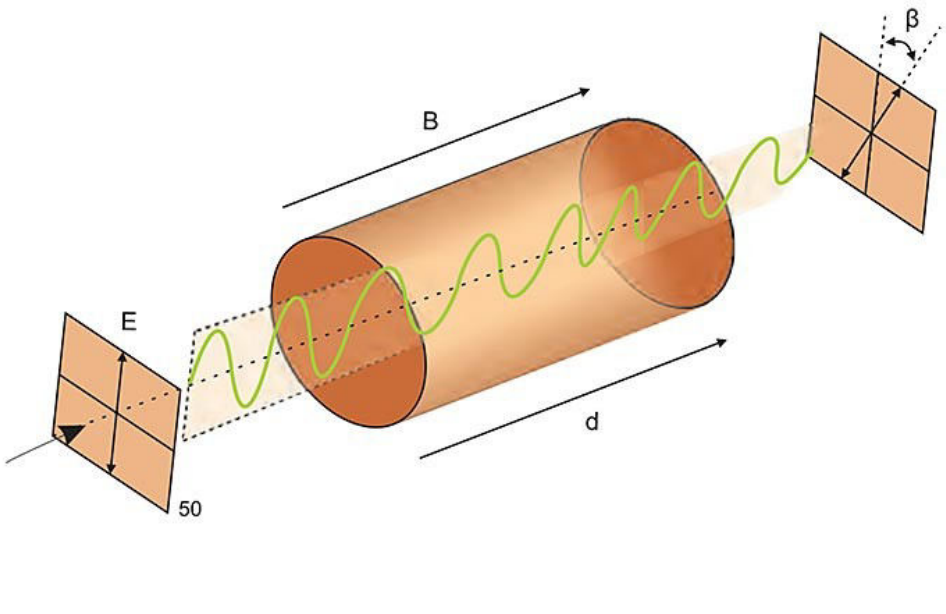

Figure 12: Polarization rotation due to the Faraday effect

Image from: https://www.holmarc.com/faraday_effect_laser.php

1.8 Optical Activity

Optical activity is the ability of a substance to rotate the plane of polarized light. Any substance or compound is said to be optically active when linearly polarized light is being rotated when passing through it. Optically active substances are classified in two types:

1. *Dextrorotatory* – These substances rotate the plane-polarized light to the right or clockwise direction. They are denoted by the prefix d or (+).

2. *Levorotatory* – The substances of this category rotate the plane-polarized light to the left or counterclockwise direction. They are designated by the prefix l or (-).

The optical rotation is the angle by which the polarization plane is rotated when polarized light traverses an optically active material. It is assigned a positive value if it is clockwise with respect to an observer facing the light source, negative if counterclockwise.

The following figure describes the phenomenon of optical rotation:

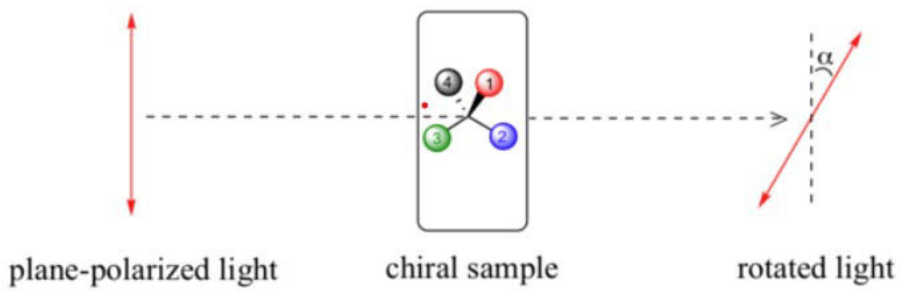

Figure 13: The effect of an optically active substance in plane-polarized light

Image from: https://chem.libretexts.org/Bookshelves/Organic_Chemistry/Book%3A_Organic_Chemistry_with_a_Biological_Emphasis_v2.0_%28Soderberg%29/03%3A_Conformations_and_Stereochemistry/3.06%3A_Optical_Activity

The intensity of optical activity is expressed in terms of a quantity called specific rotation, given by:

$$a=\frac{\theta}{l\rho} \quad \text{or} \quad \theta=\alpha l\rho \quad \textbf{(1.8.1)},$$

where α is the specific rotation, in units $\frac{degrees}{dm\frac{gr}{ml}}$, θ is the angle of optical rotation, l is the length of the light path through the sample, and **ρ** is the density of the optically active ssubstance.

1.9 Chirality

Chirality is a geometric property of asymmetry. It refers to a structure lack of symmetry elements, such mirror plane and inversion symmetry.

A configuration is considered as chiral if it can be distinguished from its mirror image. This means that, a chiral object and its mirror image, called enantiomers, cannot be superimposed to each other.
It does not take an effort to find a natural case of chirality. Our own body includes the most easily recognizable example: human hands. This should not be surprising, since the term itself originates from the Greek word "χειρ", which translates to hand. Our left hand is the mirror image of our right hand and vice versa, but when someone tries to place their right hand on top of their left hand, they immediately come to the realization that they can never coincide. The figure below clarifies this point:

Figure 14: Human hands as the perfect chirality example

Image from: http://spicyip.com/2015/09/patent-office-rejects-tofacitinib-patent-application-an-analysis-part-i.htm

From animal or sea shells to the weak nuclear force, there are countless examples of chirality found everywhere in nature. Here, we present some examples of chiral molecules we are all familiar with:

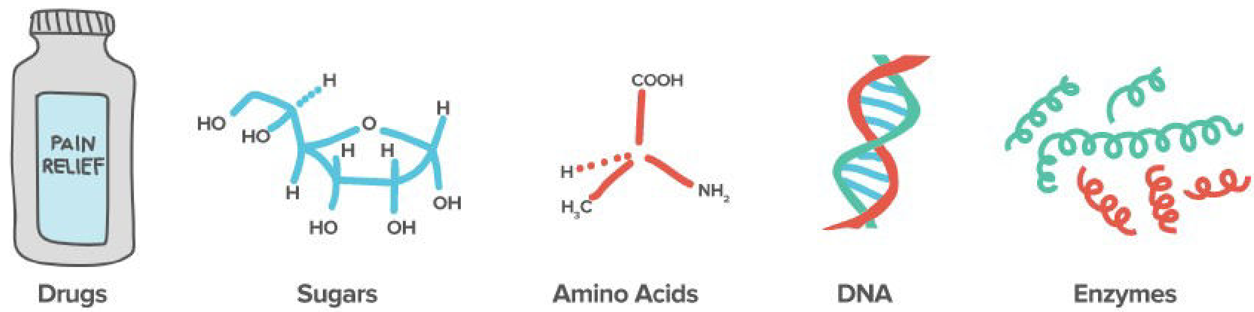

Figure 15: Examples of chiral molecules

Image from: https://www.khanacademy.org/test-prep/mcat/chemical-processes/stereochemistry/a/chiral-drugs

Chirality generates circular birefringence. Subsequently, when a beam of light passes through a chiral sample, it undergoes optical rotation. The sign of chiral rotation is dependent on the propagation direction of the beam inside the sample of interest. Schematically:

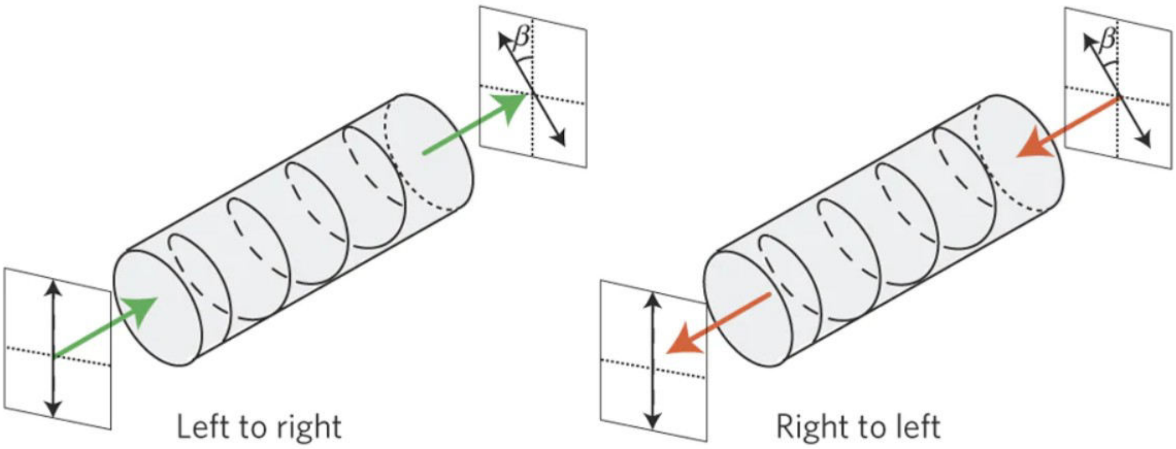

Figure 16: The dependence of the sign of chiral optical rotation on the propagation direction

Image from: https://www.fiberoptics4sale.com/blogs/wave-optics/99205446-faraday-effect

We must keep the reciprocal nature of chiral rotation in mind when designing the cavity that is going to be used in such measurements. Standing cavities are unsuitable, due to the fact that a beam of light in a cavity of this type traverses the chiral medium twice per round trip, which leads to a null value in the total chiral rotation. Thus, we tend to make use of running bow-tie cavities. Such cavities allow the beam to keep propagating in the same direction when traversing the chiral medium.

2: Experiment

2.1 Techniques

Our goal is to measure rotations in the polarization plane of light caused by chiral samples. However, such chiral rotations are particularly small, at the order of a microdegree, which makes the detection process extremely difficult. In order to enhance the obtained signal, we must increase the path length of the light through the sample. This is achieved if utilizing a four-mirror bow-tie optical cavity, which allows the beam of light to perform multiple passes through the chiral sample.

Moreover, as mentioned above, we include a 4 mm long CeF_3 magneto-optical crystal in one of our cavity's arms, to exploit the Faraday effect. When we apply a magnetic field that is parallel to the crystal, a Faraday rotation is introduced. This rotation, suppose θ_F, is notably larger than the chiral rotation, φ_C, with a difference of approximately 4 orders of magnitude. This is a tool that allows us to have a detectable signal, out of which we can derive a measurement. It also eliminates the effects of linear birefringence.

The beating frequency becomes: $\omega=\frac{(\theta_F+\varphi_C)\cdot c}{L}$ **(2.1.1)**, where c is the speed of light and L is the total length of our cavity.

The main issue is that Faraday rotation cannot be determined with precision. This can be handled nevertheless. A four-mirror bow-tie cavity can support two distinct counter-propagating beams. An additional mirror out of the cavity can lead the back reflection of the input coupler back inside the cavity, bringing in a second beam of light. These two counter-propagating beams, that we will refer to as CW (~clockwise) and CCW (~counterclockwise), perform their round trips in the cavity simultaneously, thus undergoing the exact same effects that potential sources of noise or drifts could cause. The importance of this aspect will be clarified soon.

When passing through the CeF_3 crystal, the two beams pick up a Faraday rotation of the same value and the same sign, since the Faraday effect is characterized as non-reciprocal. Their propagation through the chiral medium has quite the opposite effect. Due to the reciprocal character of chiral optical rotation, the two beams pick it up with a difference in the sign.

The effect on the beating frequency is: $\omega_{CW}=\frac{(\theta_F+\varphi_C)\cdot c}{L}$ and $\omega_{CCW}=\frac{(\theta_F-\varphi_C)\cdot c}{L}$ **(2.1.2)**.

Finally, we apply the method of magnetic reversal, which means that the direction of the magnetic field is reversed after an adequate pulse number. Therefore, we obtain a second set of beating frequencies, with a negative sign to the Faraday rotation. Each measurement includes four different signals, and so we get four different beating frequencies:

$$\omega_{CW}(\pm B)=\frac{(\pm\theta_F+\varphi_C)\cdot c}{L} \quad \text{and} \quad \omega_{CCW}(\pm B)=\frac{(\pm\theta_F-\varphi_C)\cdot c}{L} \quad \textbf{(2.1.3)}.$$

As a consequence, the chiral optical rotation can be calculated by:

$$\varphi_C=\frac{[(|\omega_{CW}(+B)|-|\omega_{CCW}(+B)|)-(|\omega_{CW}(-B)|-|\omega_{CCW}(-B)|)]\cdot L}{4c} \quad \textbf{(2.1.4)}.$$

This result proves why the aforementioned techniques were of critical importance. The introduction of a magneto-optical crystal provides us with a measurable quantity. The existence of two counter-propagating beams of light inside the cavity allows us to take advantage of the Faraday effect without the need to determine the exact value of the polarization rotation angle caused due to the crystal. Finally, magnetic reversal contributes to the elimination of various noises and enhances the presence of chiral rotation.

2.2 Setup

The laser we employ throughout our experiment is a pulsed diode laser (RLTMPL-532-500-3-19042759) of a 554 mW power, producing 5.83 nsec pulses at a repetition rate that varies from 1 to 10 kHz.

Before the light beam emitted by the laser enters the cavity, it is mode matched with the utilization of two lenses placed before the input coupler and a lens that is placed in the path of the reflection. The latter is used for a correction in the path difference the main and the back-reflected beam present.

A customized isolation system is set before the cavity to ensure the avoidance of feedback phenomena caused by the back-reflected beam, that could return back to the laser. This isolator is consists of four main parts: two polarizing beam splitters as our polarizers, a cylindrical permanent magnet and a Terbium Gallium Garnet (~TGG) crystal. The light losses of this system were reduced to a minimum with the assistance of a quarter wave plate.

Moving on to the cavity itself, two out of its four mirrors are flat anti-reflection (~AR) coated mirrors of reflectivity R_p=99.9%, and the remaining two are spherical AR coated mirrors of reflectivity Rs=99.98% and their radius of curvature is r=1.5 m. The total length of our cavity is L=3.61 m, with the smaller arm being 85 cm and the larger one being 95 cm. Potential ellipticity signs in the polarization of light were tackled using a half wave plate.

Two analyzers, one concerning the CW and one for the CCW beam are placed right after the cavity. Their transmission axes are perpendicular to the input light polarization. The output beams are focused on two photodetectors via two lenses. These photodetectors are connected to a PC and their signals are transferred to a Fast Data Acquisition Card that the PC is supplied with.

A schematic of the layout described above is depicted as follows:

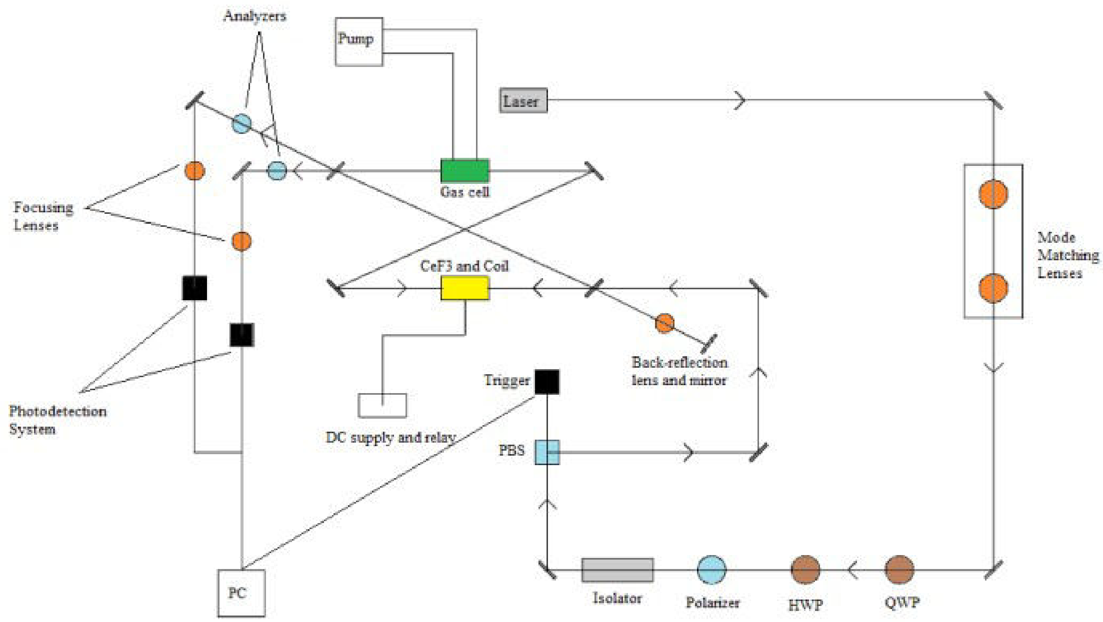

Figure 17: Experimental Setup – Scheme

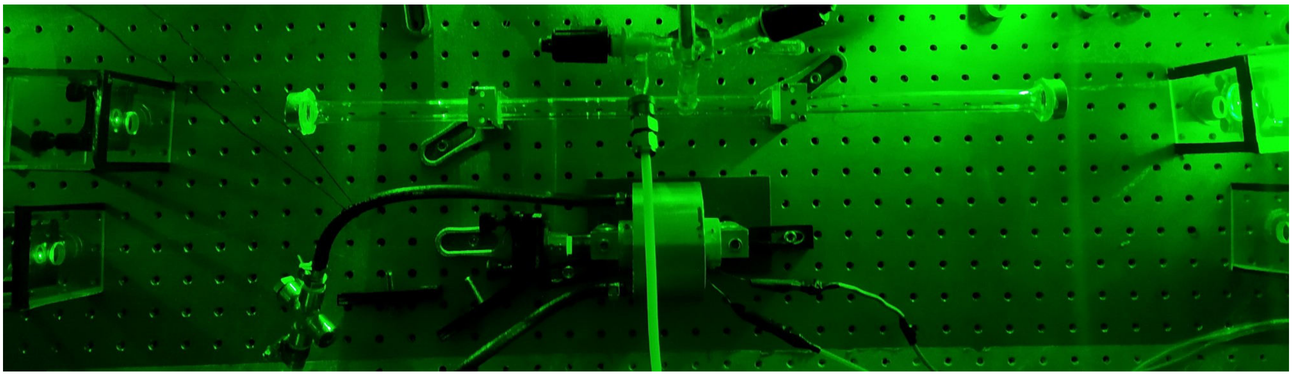

Figure 18: Experimental Setup – Photograph

The cell containing our gaseous samples has a length l=55 cm and is connected to a mechanical oil pump reaching a vacuum at the order of 10^{-2} mbar after functioning for approximately 3-5 minutes. The main part of the cell is enclosed by two high reflectivity anti-reflection coated windows. As depicted below, there is a separate cell compartment that isolates the sample, in its liquid phase, via a valve.

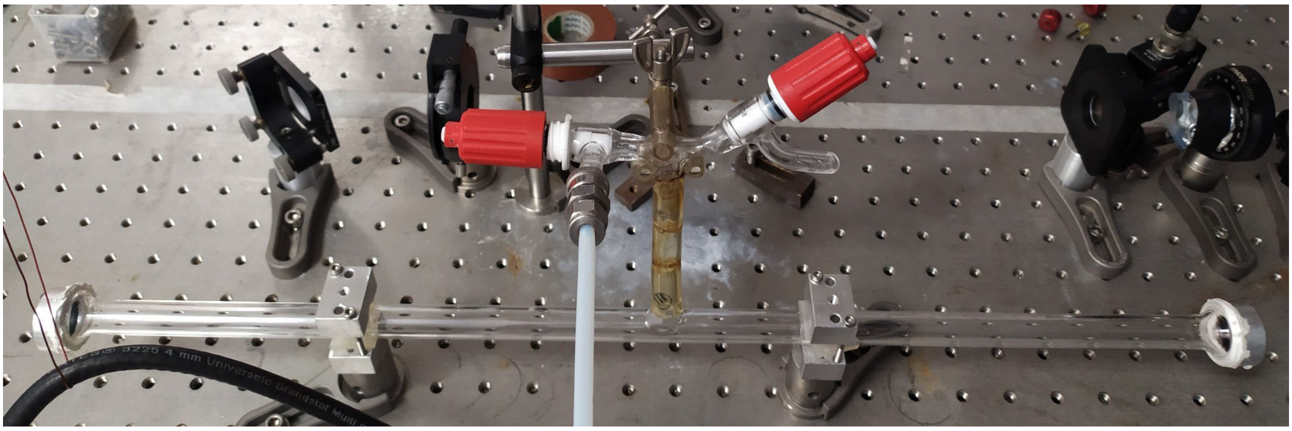

Figure 19: Gas Cell – Photograph

We have also constructed a 3 cm long, 23-layer and 30-turn coil, so as to introduce a Faraday rotation in addition to the chiral one. The diameter of the cable used in the coil construction is 1 mm. We control the current running through the coil via a DC current generator, which, furthermore, incorporates a relay that is responsible for reversing the direction of the current, after a relative PC command. The coil includes a cooling system which enables a mixture of water and ethanol to circulate its enclosure, so that its components are not affected by rising temperatures and that the crystal remains intact concerning thermal phenomena.

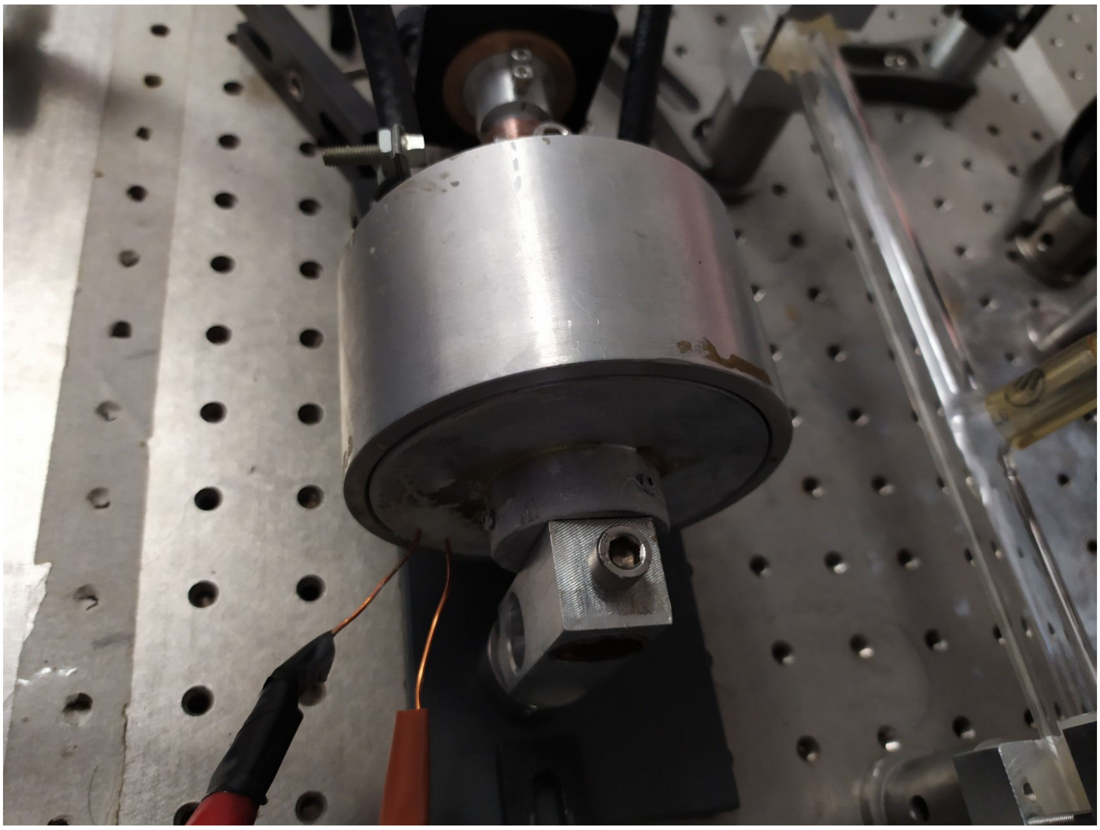

Figure 20: Coil – Photograph

2.3 Measurement Acquirement

The experimental process begins with setting up the laser to operate at a repetition rate of 10 kHz and a duty cycle of 99.984%, which is the maximum value the laser can be set to function at.

The power supply of our current generator is regulated to provide a DC current of I=7.5 A. This leads to a magnetic field of approximately 1200 G at the center of the coil, which is home to the CeF_3 magneto-optical crystal. At the same time, we initiate the operation of the coil's cooling system. We allow the plain operation of the current generator for about 15 to 20 minutes before acquiring any measurements to ensure the thermal equilibrium of the coil-crystal system, and thus avoid the interference of thermal phenomena with the process.

In order to proceed with data acquisition, we make use of the Ultrachiral Software, developed exclusively to this end, and installed in our PC. This software enables us to record three signals simultaneously, two of which are the signals of the CW and CCW beams, and the third one being the trigger. The trigger signal is obtained from a photodetector that is placed close to the point where light meets our isolator.

An image representing the Graphical User Interface of the Ultrachiral Software is included below:

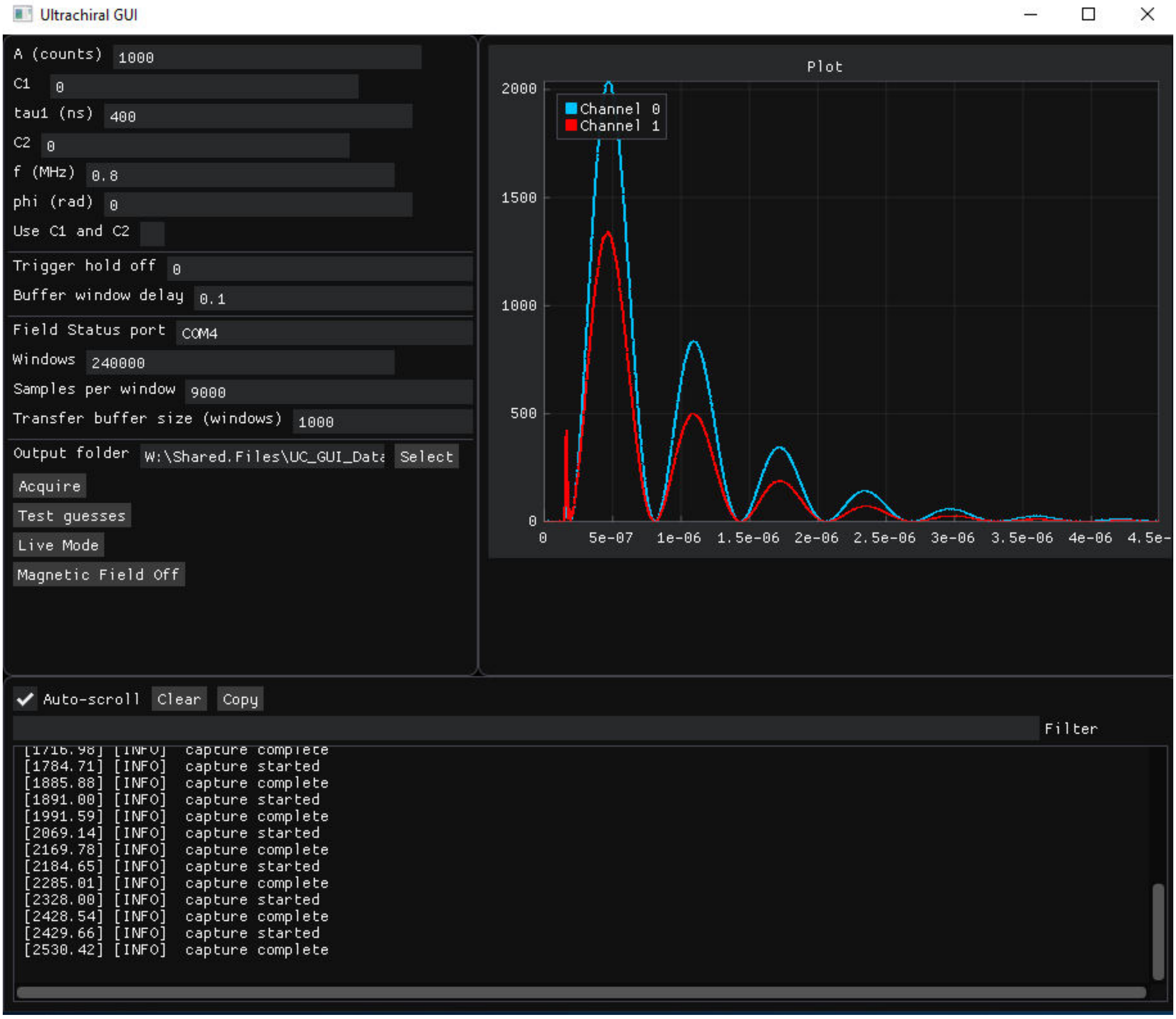

Figure 21: Ultrachiral GUI

The signal that can be observed in the GUI figure is a live representation of the signal during data acquisition: the blue curve stands for the CW beam, while the red one represents the CCW beam.

The variable numerical inputs that we choose and set before acquiring a measurement, in order of appearance in the figure above, are the following:

- Buffer Window Delay: It refers to the amount of time during which there will be no signal recording after the current direction is reversed. It is critical for the coil to have time to settle.

- Windows: The number of pulses recorded by the system throughout a complete measurement.

- Samples per Window: It is a number proportional to the amount of time (in μsec) during which a pulse's ringdown is recorded.

- Transfer Buffer Size: The number of pulses the system records and averages before the software commands the magnetic field reversal via the relay. One full measurement demands double the amount of these pulses.

The remaining inputs are set as initial guesses of these parameters, used in the fitting process of the Ultrachiral Software.

A complete measurement requires the following time:

$\tau_{measurement} = \frac{2\,tbs}{repetition\,rate} \approx 0.2\,sec$ **(2.3.1)**, where tbs stands for the transfer buffer size.

2.4 Experimental Results

After completing the aforementioned steps, we move on with our measurements. To begin with, we pump the empty cell until the vacuum reaches a value of about 10^{-2} mbar. When that limit is reached, we acquire a measurement concerning the empty cell. Then, we open the valve that connects the compartment of the cell housing the liquid Methyl Lactate, allowing vapors to fill the cell, and acquire another measurement, concerning our gaseous sample inside the cell. When the measurement is completed, we close the valve, thus isolating this compartment from the rest of the cell, and restart pumping. Then, we wait until the vacuum value returns to its previous level, and obtain a measurement concerning the empty cell.

The pressure inside the cell is measured using a Thermovac, attached to the part of the cell between the main chamber and the potentially isolated compartment. The difference in the vacuum values shown in the Thermovac in the case of the empty cell and the filled cell is several (~3) orders of magnitude.

We repeat the process mentioned above five times, and the results are presented in the following figure:

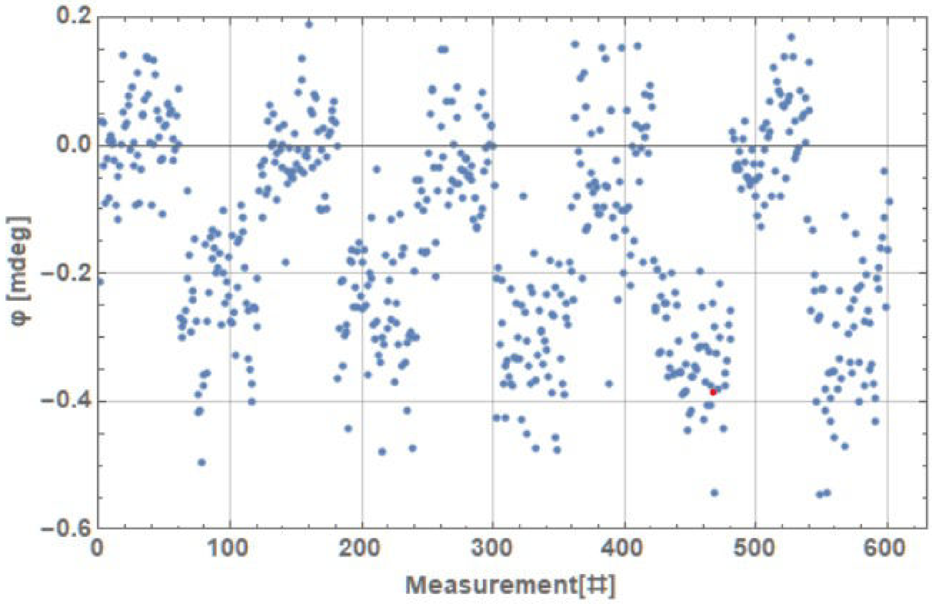

Figure 22: Chiral optical rotation angles of the empty cell and Methyl Lactate

Next up, we show the mean value the total measurement:

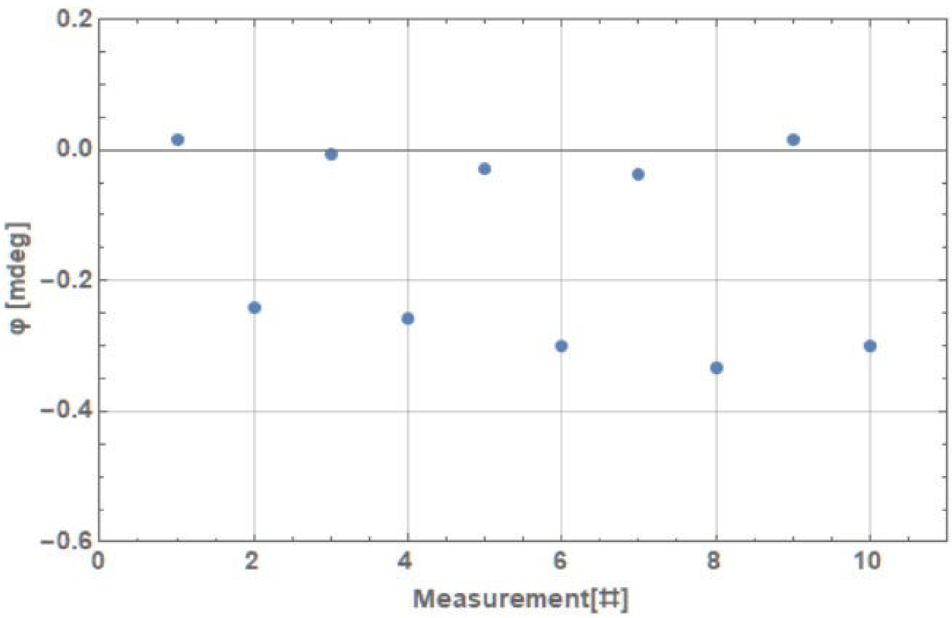

Figure 23: Mean value of chiral optical rotation angles of the empty cell and Methyl Lactate

The final result for the chiral optical rotation angle of Methyl Lactate is derived if we subtract the mean value of the measurements concerning the empty cell from the mean value of the ones concerning the filled-with-sample cell.

We get: $\varphi_c = 0.279 \pm 0.027\, mdeg$.

Applying **(1.8.1)** to find the specific rotation of Methyl Lactate yields:

$$\alpha = 2.54 \pm 0.25 \frac{deg \cdot cm^3}{dm \cdot gr}$$

Note that ρ in **(1.8.1)** is found using the Ideal Gas Law for a temperature of T=25° C.

2.5 Final Remarks

We have managed to successfully measure the particularly weak chiral optical rotation of gaseous methyl lactate samples, with a sensitivity at the order of 30 μdeg. The rotation angles characterizing such samples cannot be determined with the application of conventional methods, such as single pass measurements.

In the past, we have effectively applied our technique in various other samples, i.e. gas-phase α-pinene and liquids such as tartaric acid, lysozyme and tears.

Near future plans include measuring the chiral optical rotation of Ethyl-1-d-benzene vapor, which is a result of the overlapping between electronical and vibrational states of the molecule by breaking down the Born-Oppenheimer approximation, making it extremely weak, with an expected specific rotation of about 0.1-1 $\frac{deg\, cm^3}{dm\, gr}$. Angular measurements of ethyl-1-d-benzene vapor are the order of our current sensitivity, so we must further improve our setup in order to succeed.

These improvements will include:

- A laser with increased power, by a factor of 6
- Obtaining better optics
- Improve the operation of the relay
- Lowering the CeF_3 crystal's losses by a factor of 2 with finer coatings (~current losses: 0.2%, losses goal: 0.1%)
- More effective cooling of the coil
- Better isolation of existing vibrations

Acknowledgments

First and foremost, I would like to thank my supervisor, Prof. T. Peter Rakitzis, for giving me the opportunity to work with his group for the past year, and for introducing me to numerous research and science concepts during this time. I would like to express my genuine gratitude to him for always being willing to offer his help to me.

Furthermore, I would like to thank Dr. George Katsoprinakis for constantly being ready to assist me and share his knowledge when needed.

A sincere thank you to Mr. Michalis Xygkis, who worked on this experiment with me, making the completion of this thesis possible.

I would also like to thank Mr. Konstantinos Tazes and Mr. Michalis Koutrakis, who were part of this experiment as well.

Finally, I would like to thank Ms. Eirini Toutoudaki and Ms. Zoi Sargianni for being two such supportive lab members.

References

1. Verdeyen, J. (1995). Laser Electronics (3rd Edition)

2. Sofikitis, D., Bougas, L., Katsoprinakis, G. E., Spiliotis, A. K., Loppinet, B., & Rakitzis T. P. (2014). Evanescent-wave and ambient chiral sensing by signal-reversing cavity ringdown polarimetry. *Nature, 514*(7520), 76-79. https://doi.org/10.1038/nature13680

3. Bougas, L., Sofikitis, D., Katsoprinakis, G. E., Spiliotis, A. K., Tzallas, P., Loppinet, B., & Rakitzis T. P. (2015). Chiral cavity ring down polarimetry: Chirality and magnetometry measurements using signal reversals. *The Journal of Chemical Physics, 143*(10), 104202. https://doi.org/10.1063/1.4930109

4. Spiliotis, A. K., Xygkis, M., Klironomou, E., Kardamaki, E., Boulogiannis, G. K., Katsoprinakis, G. E., Sofikitis, D., & Rakitzis T. P. (2020). Gas-phase optical activity measurements using a compact cavity ringdown polarimeter. *Laser Physics, 30*(7), 075602. https://doi.org/10.1088/1555-6611/ab8d2e

5. Spiliotis, A. K., Xygkis, M., Klironomou, E., Kardamaki, E., Boulogiannis, G. K., Katsoprinakis, G. E., Sofikitis, D., & Rakitzis T. P. (2020). *Chemical Physics Letters* 747 137345. https://doi.org/10.1016/j.cplett.2020.137345

6. Paschotta, R. (2021, July 17). *Cavities*. 2022 RP photonics AG. https://www.rp-photonics.com/cavities.html

7. Paschotta, R. (2021b, November 28). *Gaussian Beams*. 2022 RP photonics AG. https://www.rp-photonics.com/gaussian_beams.html

8. Paschotta, R. (2021, July 17). *Birefringence*. 2022 RP photonics AG. https://www.rp-photonics.com/birefringence.html

9. Tazes, K. (2022) *Chiral sensing of gases by signal reversing cavity ringdown polarimetry.* [Master's Thesis, University of Crete]

10. Koutrakis, M. (2022) *Sensitive chiral sensing of single-drop solutions by signal-reversing cavity-ringdown polarimetry.* [Master's Thesis, University of Crete]